Cellular Signalling 60 (2019) 1–16

Contents lists available at ScienceDirect

Cellular Signalling

journal homepage: www.elsevier.com/locate/cellsig

Tumor-secreted GRP78 facilitates the migration of macrophages into tumors by promoting cytoskeleton remodeling

Xiaoqin La[a,1], Lichao Zhang[b,1], Yufei Yang[a], Hanqing Li[c], Guisheng Song[d,**], Zhuoyu Li[a,b,c,*]

[a] Institute of Biotechnology, Key Laboratory of Chemical Biology and Molecular Engineering of National Ministry of Education, Shanxi University, Taiyuan 030006, China
[b] Institutes of Biomedical Sciences, Shanxi University, Taiyuan 030006, China
[c] School of Life Science, Shanxi University, Taiyuan 030006, China
[d] Department of Medicine, University of Minnesota, MN 55455, USA

ARTICLE INFO

Keywords:
Tumor-secreted GRP78
Macrophages
Directional migration
Cytoskeleton remodeling
Ca^{2+}

ABSTRACT

Glucose-regulated protein 78 (GRP78), an important molecular chaperone in the endoplasmic reticulum, is often over-expressed in the central region of advanced tumor and acts as a promoter of tumor progression. As main immune cells in the tumor microenvironment, infiltration of abundant macrophages into advanced tumor further facilitates growth of tumor. Although has potential association between GRP78 and infiltration of macrophages, its underlying mechanisms are poorly understood. Here, we report that secreted GRP78 facilitates recruitment of macrophages into tumors both *in vitro* and *in vivo*. Further studies reveal that secreted GRP78 transports into macrophages and bound to intracellular Ca^{2+}, which lead to uneven distribution of Ca^{2+} and subsequent polarization of macrophages. The polarization of macrophages activates expression of microRNA-200b-3p. By directly targeting *RhoGDI*, miR-200b-3p stimulates the activity of RhoGTPase and ultimately leads to the distribution of GTP-Rac1 and GTP-Cdc42 in front protrusion and GTP-RhoA in rear contraction, which further results in migration of macrophages in a certain direction. Our results reveal a novel function of GRP78 to promote the recruitment of macrophages to tumor and provide a potential therapeutic target for malignancies.

1. Introduction

Glucose regulated protein 78 (GRP78), a conserved molecular chaperone protein in the endoplasmic reticulum, usually facilitates proper folding and assembly of proteins in normal cells [1,2]. Moreover, it usually binds to calcium and serves as a sensor of calcium homeostasis in ER [3]. In advanced tumors, growth rate of tumor cells exceeds the blood supply, which leads to the tumor microenvironment characterized by glucose deprivation, acidosis and hypoxia [1,4]. These adverse conditions further drive expression of GRP78 in various types of tumors, including colon cancer, breast cancer, liver cancer, stomach cancer, esophageal cancer, brain cancer, prostate cancer and melanoma [5–7]. Accumulating evidence has demonstrated that over-expression of GRP78 leads to tumor resistance to apoptosis, immune escape, drug resistance, metastasis and angiogenesis [8,9]. All these findings indicate that GRP78 plays a vital role in promoting progression of tumor.

Increased intracellular GRP78 may exceed the retention capacity of the KDEL recovery system, which leads to the escape of GRP78 from ER and secretion from tumor cells into the tumor microenvironment [10]. Tumor-secreted GRP78 induces pro-survival signals and subsequently blocks the antiangiogenic activity of bortezomib *via* phosphorylation of extracellular signal–related kinase and inhibition of p53-mediated expression of pro-apoptotic Bok and Noxa proteins in endothelial cells [11], and it differentiates bone marrow-derived mesenchymal stem cells (BMSCs) into cancer-associated fibroblasts (CAFs) through activating TGF-β/Smad signaling pathway in an autocrine/paracrine manner [12]. Together, GRP78 has a potent transform function in the tumor microenvironment (TME).

Monocytes in peripheral blood are incompletely differentiated cells that are very sensitive to changes in the microenvironment. When these

Abbreviations: GRP78, Glucose-regulated protein 78; TAM, tumor-associated macrophages; RhoGDI, Rho GDP dissociation inhibitor alpha; TCM, Tumor conditioned medium

* Correspondence to: Z. Li, Institute of Biotechnology, Key Laboratory of Chemical Biology and Molecular Engineering of National Ministry of Education, Shanxi University, Taiyuan 030006, China.
** Correspondence to: G. Song, Division of Gastroenterology, Hepatology and Nutrition, University of Minnesota, 516 Delaware Street SE, Minneapolis, MN 55455, USA.
E-mail addresses: gsong@umn.edu (G. Song), lzy@sxu.edu.cn (Z. Li).
[1] These authors contributed equally.

https://doi.org/10.1016/j.cellsig.2019.04.004
Received 11 February 2019; Received in revised form 4 April 2019; Accepted 4 April 2019
Available online 05 April 2019
0898-6568/

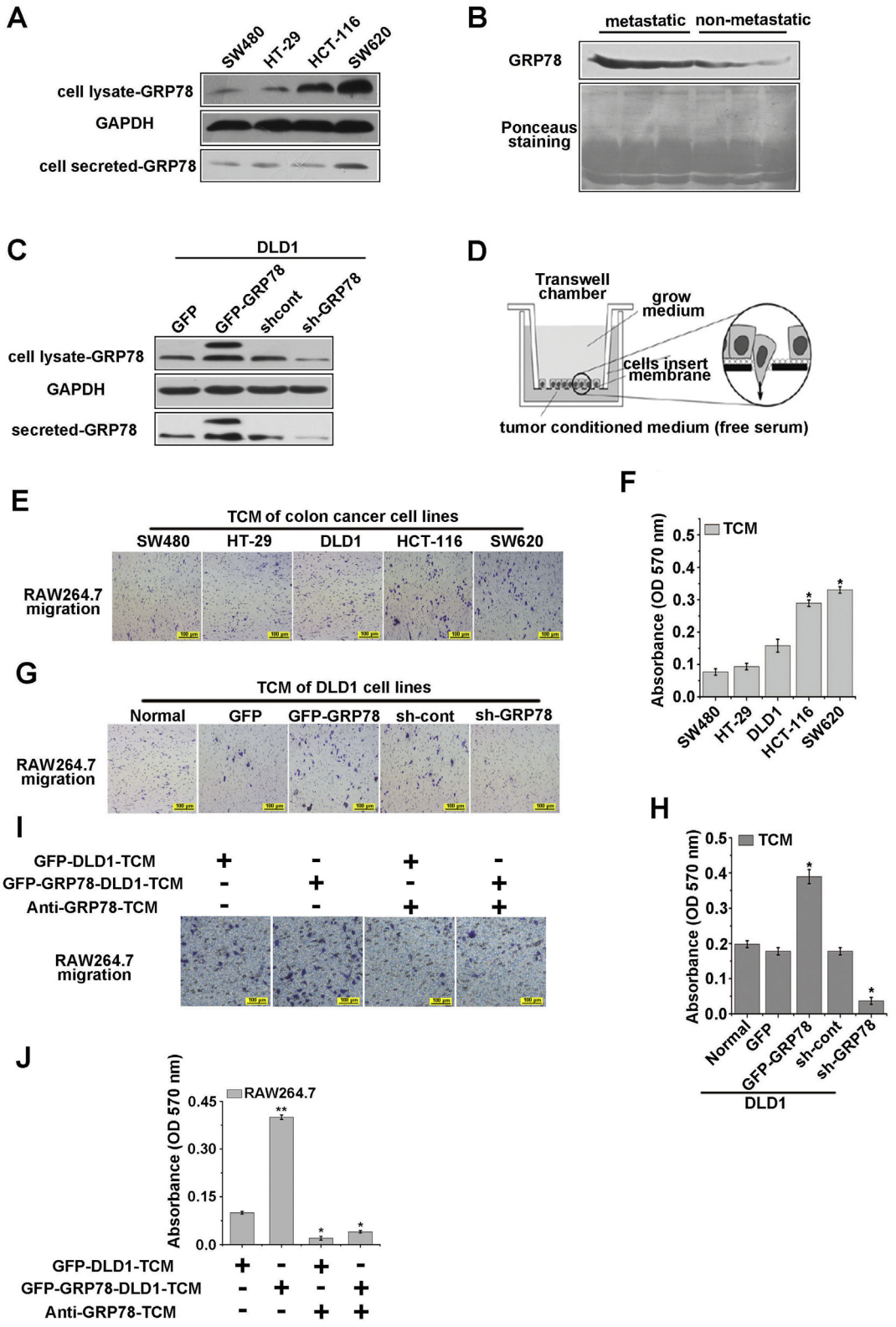

Fig. 1. Secreted GRP78 plays a critical role in RAW264.7 and THP-1 cells migration.
(A) Protein levels of GRP78 in supernatants and cell lysates in HT-29, SW480, HCT-116 and SW620 cells. All cells were cultured in serum-free medium for 48 h. Supernatants and cells were collected and subjected to western blot analysis. (B) Western blot analysis of GRP78 in serums of different colorectal cancer patients. (C) Immunoblots of GRP78 in the whole-cell lysates and culture supernatants of DLD1 cells stably expressing GFP and GRP78-GFP or GRP78-knockdown. (D) The schematic of Transwell co-culture system was shown. (E and F) Transwell assays were applied to evaluate the effects of SW480, HT-29, DLD1, HCT-116 and SW620 conditioned medium on RAW264.7 cells migration, and the bar graph indicated the cell motility that shown in E, $^{*}p < .05$. (G and H) Transwell assays were used to evaluate the effects of TCM in DLD1 cells that stably knocking down or over-expressing GRP78 on RAW264.7 cell migration, and the bar graph represented the cell motility, $^{*}p < .05$. (I and J) After neutralizing GRP78 in TCM with antibody, TCM was applied to evaluate the effect on RAW264.7 migration using a Transwell assay, scale bar: 100 μm, $^{*}p < .05$.

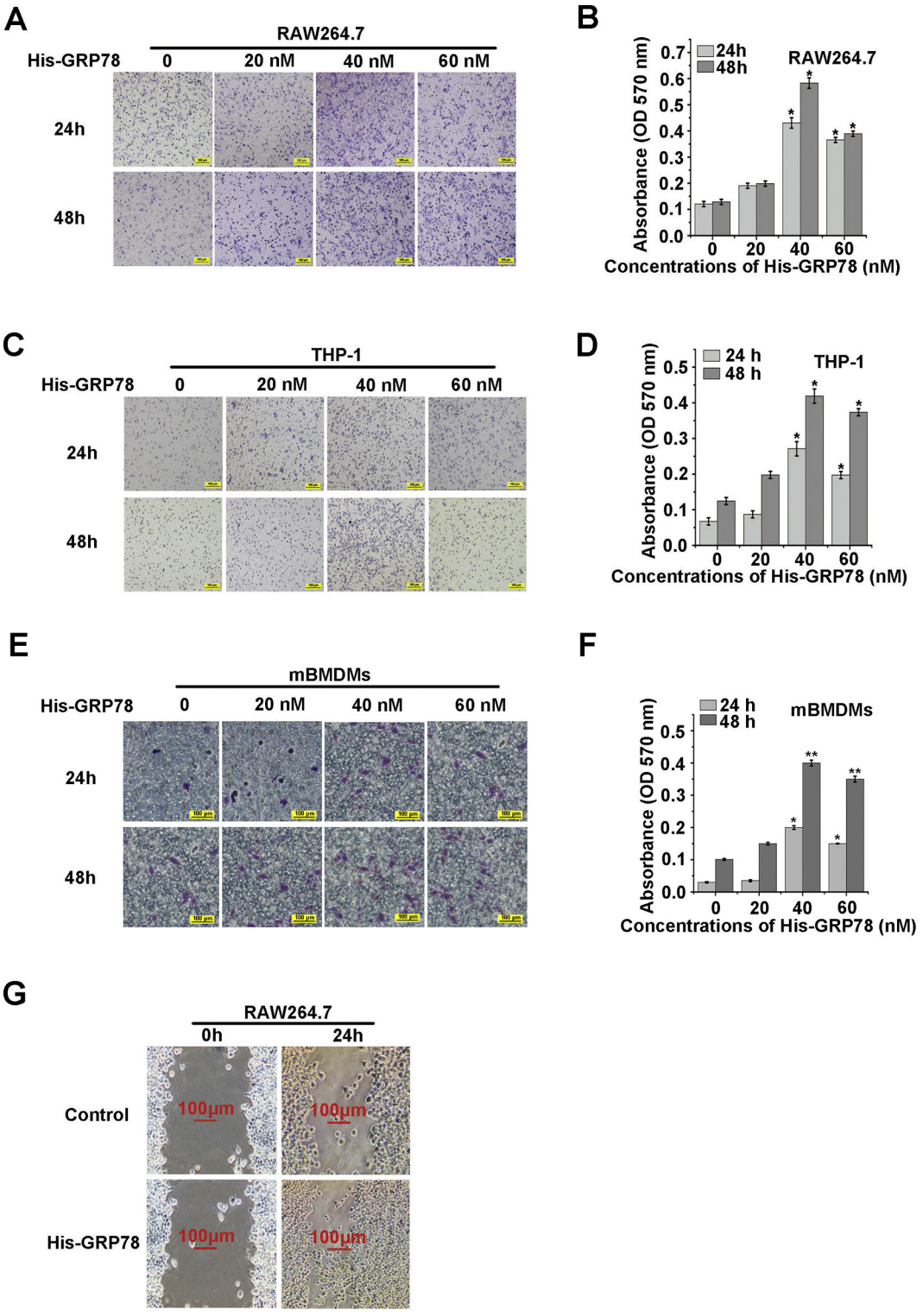

Fig. 2. Secreted GRP78 promotes migration of macrophages.
(A and B) Transwell assay was used to evaluate the effects of different concentrations of His-GRP78 on RAW264.7 cells migration for various points of time, and the bar graph represented the RAW264.7 cells migration that was shown in A, scale bar: 100 μm, $^{*}p < .05$. (C and D) Transwell assay was applied to evaluate the effect of different concentrations of His-GRP78 on THP-1 cells migration, and the bar graph represented the THP-1 cells migration that was shown in C. $^{*}p < .05$. (E and F) Transwell assay was applied to evaluate the effect of different concentrations of His-GRP78 on mBMDMs migration and the bar graph represented the mBMDMs cells migration that was shown in E. $^{*}p < .05$, $^{**}p < .01$. (G) Wound healing assay was used to detect the effect of His-GRP78 on RAW264.7 cells migration. Red scale bars in the panels represented 100 μm. (For interpretation of the references to colour in this figure legend, the reader is referred to the web version of this article.)

monocytes are recruited into specific tissues, they rapidly differentiate into mature macrophages that have specific functions in tumor progression [13]. With the progression of tumors, the tumor microenvironment is gradually stabilized in the advanced stages. These mononuclear/macrophages are recruited to tumor tissues by various factors that exist in the tumor microenvironment and subsequently

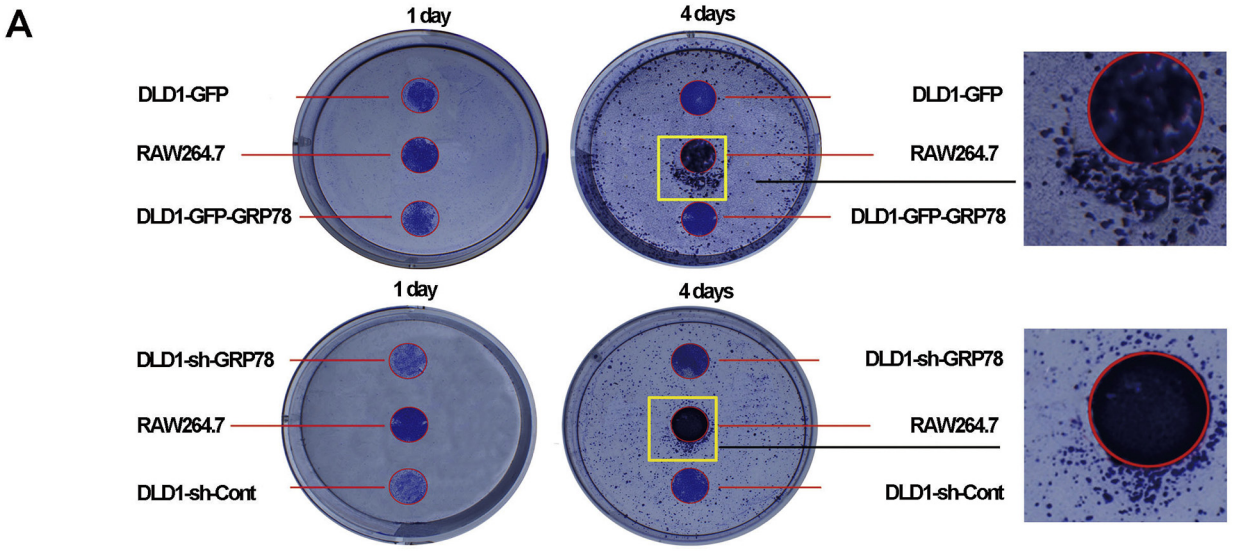

C

The distance of RAW264.7 migration (mm)

Cell lines	Distance (mm)
DLD1-GFP	0.9 ± 0.1
DLD1-GFP-GRP78	4.5 ± 0.1
DLD1-sh-GRP78	1.2 ± 0.1
DLD1-sh-cont	3.0 ± 0.1

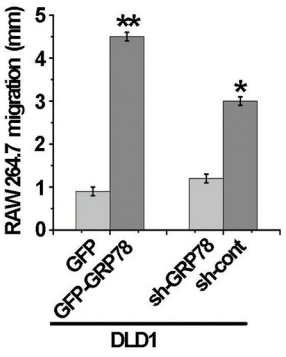

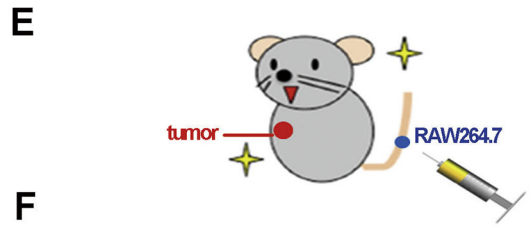

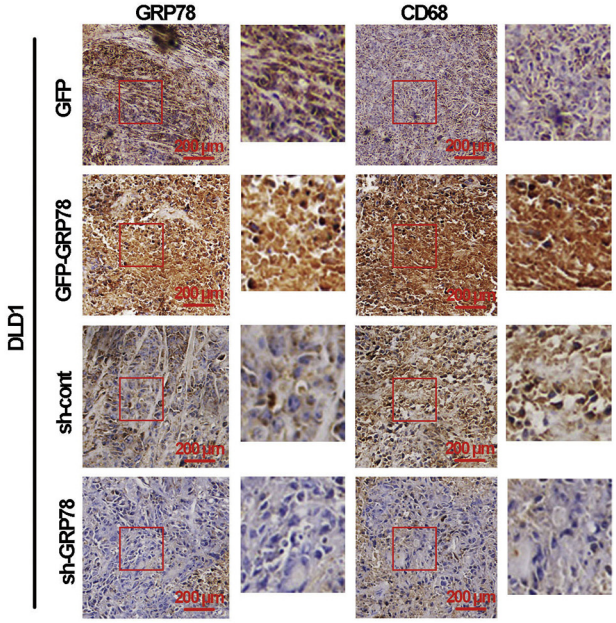

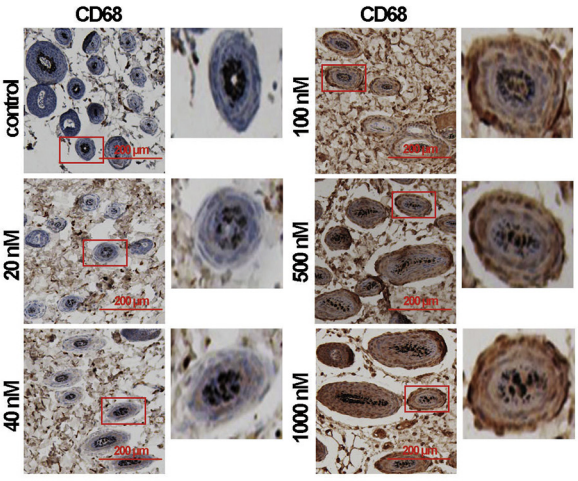

(caption on next page)

Fig. 3. Secreted GRP78 promotes directional migration of macrophages.
(A) The migration of RAW264.7 was detected by Crystal violet staining. (B) The schematic diagram of experimental design. (C) The distance of RAW264.7 cells migration toward different GRP78 secretion. (D) The bar graph represented the distance of RAW264.7 migration, $^{*}p < .05$, $^{**}p < .01$. (E and F) IHC analysis detected RAW264.7 infiltration in the tumor tissues (F) and the schematic diagram of experimental design was shown in E. (G and H) IHC was used to detect the infiltration of macrophage after matrigel and different concentrations of His-GRP78 mixture injected into mice axillary skin. Representative images were presented (H) and the schematic diagram of experimental design was shown in G. (For interpretation of the references to colour in this figure legend, the reader is referred to the web version of this article.)

become tumor-associated macrophages (TAMs) [14]. Casazza A et al. reported that hypoxia promoted the entry of macrophages into the hypoxic areas of tumors by activating Sema3A/Nrp1/PlexinA1/PlexinA4 signaling [15]. Sica A and Grimshaw MJ et al. also revealed that hypoxia impaired expression of the macrophage-surface chemokine receptors (CCR2 and CCR5) by inhibiting ERK1/2 and p38/MAPK signaling, which further reduced the sensitivity of macrophages to chemotactic signals and ultimately led to the accumulation of macrophages in hypoxic sites [16,17]. As a result, abundant macrophage infiltration becomes a common feature of tumors [18,19]. These TAMs function as the promoter of tumor progression. For example, Hagemann T et al. revealed that TAM secreted a large number of proteases, such as cathepsin, urokinase-type plasmin (uPA), matrix metalloproteinases (MMPs) and serine proteases, which degraded tumor extracellular matrix and helped tumor cells break through the basement membrane and metastasize [20].

Based on these established findings, we speculate that TAMs and GRP78 have similar function of promoting tumor development; they usually gather in the hypoxic areas of tumor tissues; and TAMs and secretion of GRP78 occur in the advanced stage of tumor. Given the "coincidence" of TAMs and GRP78 in the function, stage of tumor development and location in the tumor, we hypothesize that GRP78 is able to facilitate the infiltration of macrophages to tumors.

In this study, we observed that migration of macrophage toward secreted GRP78 in a concentration-dependent fashion. High levels of secreted GRP78 promoted the entry of more GRP78 into macrophages and bound to intracellular Ca^{2+}. The uneven distribution of intracellular free Ca^{2+} exhibited an uneven subcellular distribution further led to the polarity of macrophages. In this study, we determined the mechanism(s) and unknown signaling pathways by which secretion of GRP78 facilitated the infiltration of macrophages and evaluated the potential of GRP78 as a therapeutic target for human malignancies.

2. Materials and methods

2.1. Reagents and antibodies

RPMI-1640 medium, DMEM medium, DMEM/F-12 1:1 medium and fetal bovine serum (FBS) were purchased from GIBCO (Grand Island, USA). Fluo-3 AM was obtained from Beyotime (Shanghai, China). Rhodamine was obtained from Cytoskeleton, Inc. (Colorado, USA). The active integrin-β1 (12G10) (Catalog: MAB2247) antibody was purchased from Sigma-Aldrich (Missouri, USA). Antibody for integrin-β1 (Catalog: 4706) were purchased from Cell Signaling Technology (Beverly, USA). Actin antibody (Catalog: M20011) was from Abmart (Shanghai, China). Antibodies against MMP-2 (Catalog: BS1236), MMP-9 (Catalog: BS1241), FAK (Catalog: BS9850M), p-FAK (Tyr397) (Catalog: BS4617) were purchased from Bioworld Technology (Minneapolis, USA). Antibodies for RhoGDI (Catalog: 10509–1-Ig), RhoA (Catalog: 10749–1-AP), Rac 1 (Catalog: 24072–1-AP), Cdc42 (Catalog: 10155–1-AP) and Fibronectin (Catalog: 66042–1-Ig) and GAPDH (Catalog: 60004–1-Ig) were obtained from Proteintech (Chicago, USA).

2.2. Serum samples of colon cancer patients

Thiry-two serum samples from colon cancer patients (16 non-metastatic patients and 16 metastatic patients) were gifted by Shanxi Provincial People's Hospital. Levels of GRP78 were measured by western blot.

2.3. Macrophage isolation from the murine bone marrow

Murine bone marrow derived macrophages (mBMDMs) were isolated according to the method of Rios et al. [21].

2.4. Cell culture

Human colon carcinoma DLD1 and monocytes THP-1 cell lines were obtained from the American Type Culture Collection and cultured in RPMI-1640 medium. Human colon cancer HCT-116, HT-29, SW480 and SW620 cell lines were cultured in DMEM/F12 1:1 medium. The murine macrophage RAW264.7 was cultured in DMEM medium. All media were supplemented with 10% FBS and 1% penicillin-streptomycin. All cell lines are cultured in a humidified tissue culture incubator containing 5% CO_2 at 37 °C.

2.5. Lentivirus infection

Human GRP78 cDNA (Gene ID: 3309) and GRP78 shRNAs (GRP78 shRNA sequence:5′-CCGGGAGCGCATTGATACTAGAAATCTCGAGATTTCTAGTATCAATGCGCTCTTTTTG-3′ and the negative control sequence: 5′-CCGGCCTAAGGTTAAGTCGCCCTCGCTCGAGCGAGGGCGACTTAACCTTAGG-3′) were subcloned into the lentiviral expressing vectors pLVX-AcGFP-N1 and pLKO.1-Puro, respectively. GRP78 expression/shRNA plasmids, psPAX2 and pMD2.G were co-transfected into 293 T cells using the HET KIT (BioWit) at 15:10:5 μg (10-cm dish). Media containing virus was collected after transfection 48 h and then concentrated using 30 kDa ultrafiltration membranes (Millipore) and sterile filtered using 0.45 μm ultrafiltration membranes. DLD1 cells were infected with the viruses in the presence of polybrene (8 μg/mL) for 48 h, and then subjected to selection by 5 μg/mL puromycin for 2 weeks.

2.6. Construction, expression, purification of His-GRP78

To mimic the secreted GRP78, recombinant pET-28a-GRP78 (named His-GRP78) were constructed, and the purification procedure was performed as our previously described [22].

2.7. Cell migration assay

For wound-healing migration assays, cells were seeded in 12-well plates for 24 h, and a 200 μL pipette tip was used to scratch the cells. After washing with phosphate-buffered saline (PBS), cells were cultured in DMEM medium for another 24 h in the presence of His-GRP78. Wounds were observed under a microscope and photographed.

For the transwell migration assay, 2×10^4 RAW264.7 cells or THP-1 cells in 200 μL of the medium were seeded into the upper chambers (consisted of polycarbonate filters, 8 μm pore size) of Transwell (Millipore). Tumor cells-conditioned medium or DMEM medium containing different concentrations of His-GRP78 was added to the bottom chamber. After incubation for 24 h, cells remaining on the upper membrane were removed with a cotton swab, while cells that had

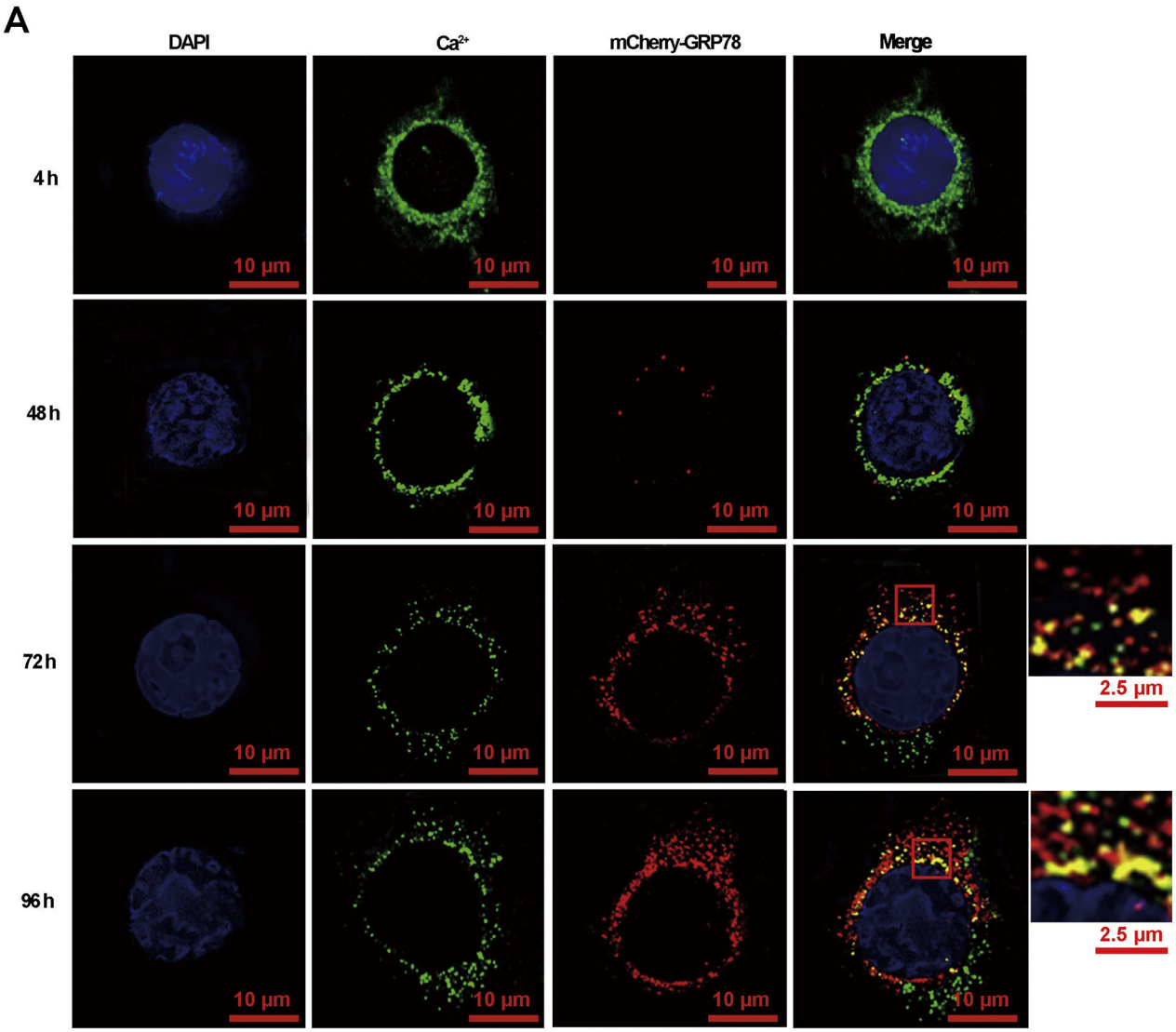

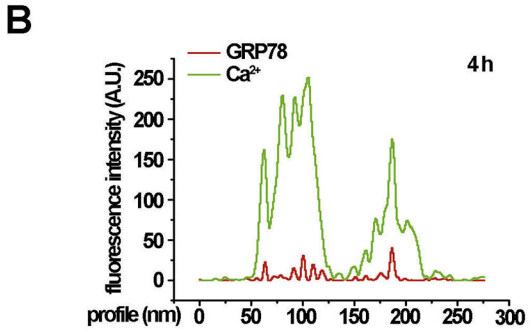

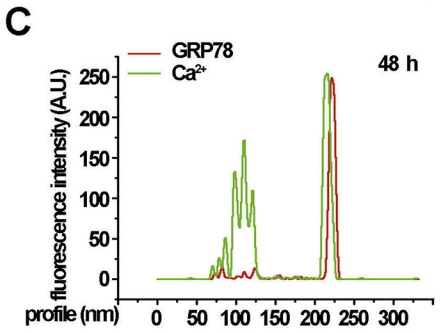

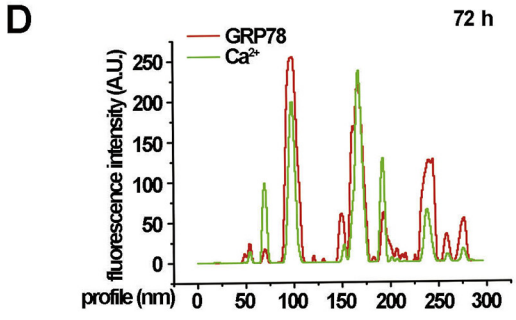

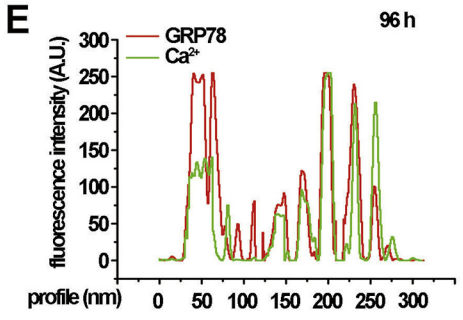

(caption on next page)

Fig. 4. Intracellular Ca^{2+} combines with GRP78.
(A) Co-localization analysis of GRP78 and Ca^{2+} in the presence of GRP78 gradient in RAW264.7 cells for different lengths of time. The schematic diagram of experimental design as showed in Fig. 2B. 4×10^4 cells (DLD1-mCherry/DLD1-mCherry-GRP78) were seed on both side cycles, 5×10^3 RAW264.7 cells were seed on the middle cycle. The entry of secreted mCherry-GRP78 into macrophages and the changes of Ca^{2+} after 4, 48, 72 and 96 h were observed. Standard confocal sections of RAW264.7 cells stained with Ca^{2+} probe (green) to mark intracellular Ca^{2+}, and DAPI (blue) to mark nucleus. Scale bars, 10 μm. (B-E) Line-scan quantifications for the indicated lines drawn across the peri-nuclear region in (A) illustrated that tumor-secreted mCherry-GRP78 combined with intracellular Ca^{2+} in RAW264.7 cells. (For interpretation of the references to colour in this figure legend, the reader is referred to the web version of this article.)

migrated through the membrane were fixed in formaldehyde, stained with crystal violet and counted using an Olympus fluorescence microscope (Tokyo, Japan).

2.8. Cell adhesion assay

For cell-matrix adhesion assays, 96-well plates were coated with rat tail collagen following adding 10^4 cells into the well. The plates were incubated at 37 °C for 30 min, 60 min, 120 min, 180 min and 360 min. After incubation, non-adherent cells were removed by PBS washing, and the adherent cells were fixed with 4% paraformaldehyde solution and stained with crystal violet (1%). After removing the excess dye, intracellular stain was solubilized with 1% SDS for absorbance analysis at 570 nm. All experiments were repeated three times.

2.9. Directional migration assay of RAW264.7 cells

Three same-size circles were drawn at the bottom of each well of a six-well plate and the distance should be the same among three circles. The tails of the yellow tip were cut and sterilized, and placed on the three circles of six-well plate. Two cell lines (the same number of cells) were seeded the first and the third circles and RAW264.7 cells were seeded the middle cycle. To prevent the cells from spreading out of the circle, the six-well plate should be placed in the cell culture incubator carefully. After attachment of the cells, the circles were taken by aseptic operation.

For the crystal violet staining assays, 2×10^4 cells (DLD1-GFP/DLD1-GFP-GRP78 or DLD1-sh-Cont/DLD1-sh-GRP78) were seeded on both side cycles, 4×10^4 RAW264.7 cells were seed on the middle cycle.

In order to observe the direction of cytoskeleton, a small corner on one side of the 24∗24 mm glass slides was knocked off, and then these slides were placed on a six-well plate. Meanwhile, three same-size circles were drawn at the bottom of each well of a six-well plate. 4×10^4 lenti-GRP78/DLD1 cells were seeded on circles that close to a glass slide with a missing corner and 4×10^4 lenti-vector/DLD1 cells were seeded on the other side cycles, which formed the concentration gradient of secreted GRP78. 5×10^3 RAW264.7 cells were seeded on the middle cycles on 24∗24 mm glass slides for 4 h, 48 h, 72 h and 96 h, respectively. After reaching time points, the slides were taken out, and the direction of the cytoskeleton change was observed by Phalloidin staining (red).

2.10. Xenograft tumor assays

Female BALB/c nude mice (4-week-old, $n = 40$) and male C57BL/6 (7-week-old, $n = 50$) were purchased from China Institute for Radiation Protection (Peking, China). All animal experiments conducted in this study were approved by the Institutional Animal Care and Use Committee of Shanxi University (Taiyuan, China). All of the experimental procedures were performed in accordance with the protocols and ethical regulations approved by the Institutional Animal Care and Use Committee of Shanxi University (Taiyuan, China).

For xenograft tumor assay, 40 female immunocompromised (nu/nu) mice were randomly divided into four groups ($n = 10$). Equal amounts (2×10^6) of DLD1 cells expressing the GFP/GFP-GRP78 or sh-cont/sh-GRP78 were re-suspended in 200 μL of PBS buffer and injected into the subcutis of mice. Once subcutaneous tumors were formed, 1×10^6 RAW264.7 cells were injected into the mice by tail vein weekly for 1 month. Then mice were euthanized, and tumors were excised and analyzed by immunohistochemistry.

For mice axillary skin injection assays, 50 male C57BL/6 mice were randomly divided into five groups ($n = 10$), and the matrigel was diluted with DMEM at 1:4. In the first group, 250 μL of cold PBS mixed with 250 μL matrigel (BD Bioscience) was injected into the armpits of each mouse (500 μL mixture each mouse). In the remaining four groups of mice, 250 μL of cold PBS containing various concentrations of His-GRP78 (20 nM, 100 nM, 500 nM, and 1000 nM) mixed with 250 μL matrigel was injected into the armpits of each mouse (500 μL mixture each mouse). According to this operation, it is injected once a week for 4 consecutive injections. A month later, the blocky matrigel were harvested and examined by immunohistochemistry.

2.11. Gelatin zymography

To investigate the gelatinase activity of MMPs, the gelatin zymography was performed. RAW264.7 cells cultured in serum-free DMEM media were treated by His-GRP78 for 24 h and then cell supernatants were collected. Gelatin zymography was carried out by subjecting conditioned media samples to 10% SDS-PAGE containing 1 mg/mL of gelatin. MMPs were activated by incubation at 37 °C for 24 h. Gels were then eluted with 12.5 mL Triton X-100, 3.03 g Tris, 0.277 g $CaCl_2$, 5 μL of 100 mM $ZnCl_2$ dissolved in 500 mL ddH_2O (elute 4 times, 15 min each time), rinsed with 3.03 g Tris, 0.277 g $CaCl_2$, 5 μL of 100 mM $ZnCl_2$ dissolved in 500 mL ddH_2O (rinse 2 times, 20 min each time), incubated with 100 mL rinse containing 0.02 g Brij (incubate 48 h at 37 °C), stained 3 h with 0.25% Coomassie brilliant blue R-250 diluted in 30% methanol and 10% acetic acid, decolored was from decoloring solution A (30% methanol and 10% acetic acid, 0.5 h), B (20% methanol and 10% acetic acid, 1 h) to C (30% methanol and 10% acetic acid, 2 h). The transparent bands indicative of degrading activity, were scanned by using the VilberLourmat Imaging and Gel Documentation System (VilberLourmat, France).

2.12. F-actin assay

F-actin is insoluble, whereas G-actin is soluble. RAW264.7 cells were lysed by cold lysis buffer (10 mM K_2HPO_4, 100 mM NaF, 50 mM KCl, 2 mM $MgCl_2$, 1 mM EGTA, 0.2 mM dithiothreitol, 0.5% Triton X-100 and 1 M sucrose, pH 7.0) and then centrifuged at 15,000 $\times g$ for 30 min. The supernatant was used for measurement of soluble actin (G-actin). To measure F-actin, the pellet was re-suspended in lysis buffer plus another equal volume of cold lysis buffer (1.5 mM guanidine hydrochloride, 1 M sodium acetate, 1 mM $CaCl_2$, 1 mM ATP, and 20 mM Tris–HCl, pH 7.5) and incubated on ice for 1 h to depolymerize F-actin, with gentle mixing every 15 min. The samples were centrifuged at 15,000 $\times g$ for 30 min and this supernatant was also used to measure actin (as a reflection of insoluble F-actin). Samples from the pellet (F-actin) fractions were loaded and analyzed by western blot.

Phalloidin has a high affinity to F-actin, thus F-actin content could be measured by rhodamine-phalloidin labeling method. In detail, RAW264.7 cells were treated with His-GRP78 for the indicated period of time, and fixed with 4% paraformaldehyde for 30 min, permeabilized with 0.1% Triton X-100 for 20 min, and incubated with rhodamine-

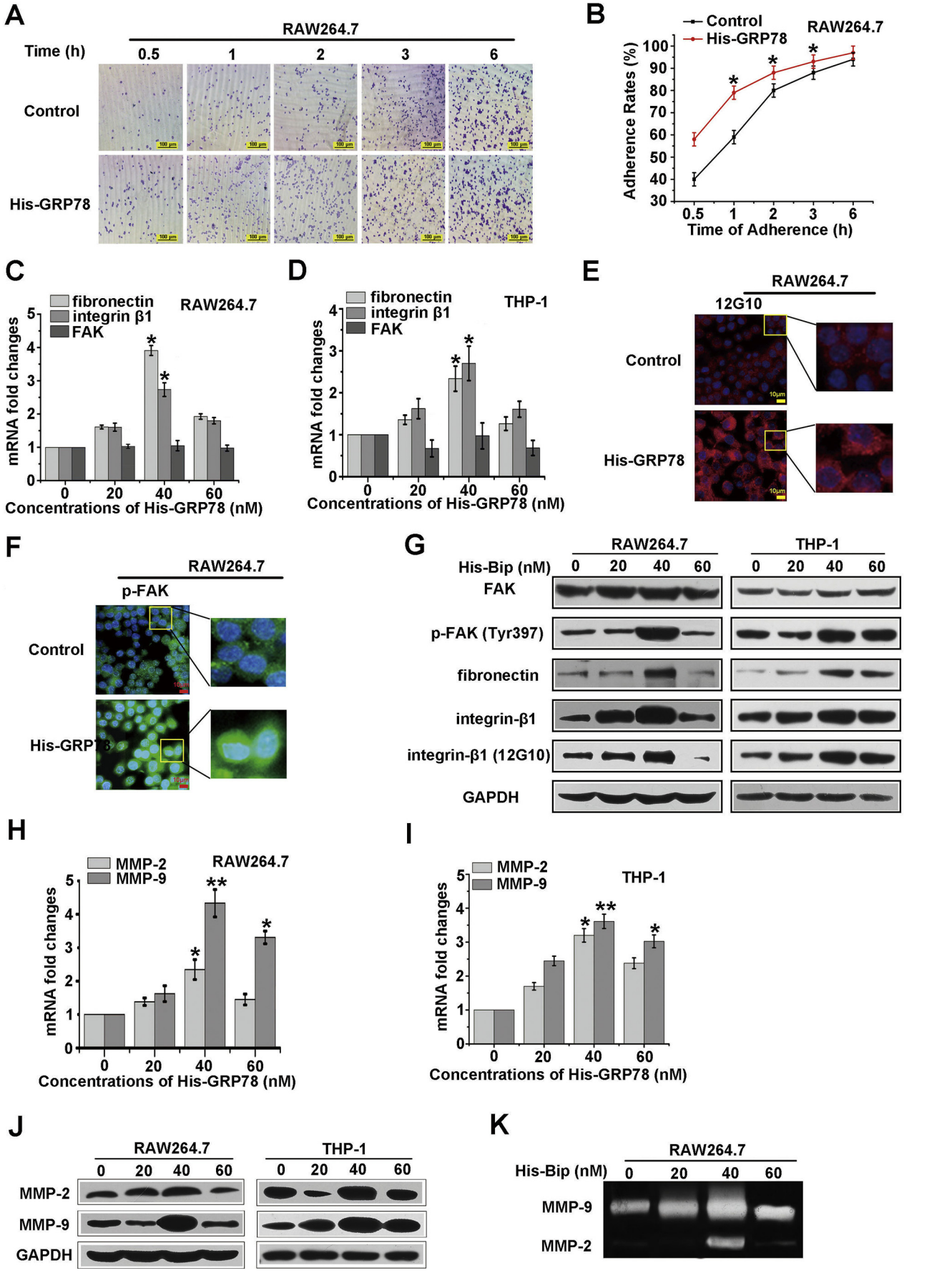

(caption on next page)

Fig. 5. The polarized cell enhances ECM adhesion and extracellular matrix degradation in RAW264.7 cells.
(A) Illustration of the ability of adhesion by bright-field microscope images. RAW264.7 cells were treated His-GRP78 for 0.5 h, 1 h, 2 h, 3 h and 6 h. Then the crystal violet adhesion assay was performed. (B) The statistical graph of cell adhesion rates, $^{*}p < .05$ was *versus* control group. (C and D) qPCR were used to detect the relative mRNA levels of fibronectin, integrin-β1 and FAK in RAW264.7 and THP-1cells treated with a serious concentrations of His-GRP78 for 24 h. The expression levels were normalized to GAPDH, $^{*}p < .05$ and $^{**}p < .01$ *versus* control group. (E and F) Immunofluorescence staining of active integrin-β1 (12G10) and p-FAK in RAW264.7 cells with or without His-GRP78 treatment. (G) Western blot of FAK, p-FAK, fibronectin, integrin-β1 and active integrin-β1 in RAW264.7 and THP-1 cells with or without His-GRP78 treatment. (H and I) qPCR were used to detect the relative mRNA levels of MMP-2 and MMP-9 in His-GRP78-treated RAW264.7 and THP-1 cells. The expression levels were normalized to GAPDH. $^{*}p < .05$, $^{**}p < .01$ were *versus* control group. (J) Western blot of MMP-2 and MMP-9 in RAW264.7 and THP-1 cells with or without His-GRP78 treatment. Mouse anti-GAPDH antibody was used as a loading control. (K) Gelatin zymography assay was used to evaluate the secretion of MMP-2 and MMP-9 in RAW264.7 cells treated with His-GRP78 at different concentrations. (For interpretation of the references to colour in this figure legend, the reader is referred to the web version of this article.)

phalloidin for 1 h. Next, 2 mL of pre-cooled HPLC grade methanol were added and placed in −20 °C for 30 min. Then the cells were scraped off, and the culture dishes were washed with 0.5 mL of methanol. After washes, bound phalloidin was extracted with methanol at −20 °C. After 12 h, the methanol suspension was separated by 2000 rpm for 15 min, and F-actin content was measured by fluorescence spectrophotometer with an excitation wavelength of 540 nm and an emission wavelength of 565 nm. Each experiment was performed in triplicate.

2.13. GTPase assay

RhoA, Rac1 and Cdc42 activation assays were performed by using small GTPase activation assay kits (Cytoskeleton, CO, USA) according to the manufacture's protocol. Briefly, RAW264.7 cells were lysed using the provided buffer. Total RhoA, Rac1 and Cdc42 levels were determined by western blot analysis of 50 μg of total protein. For the determination of activation status, 800 μg of the protein lysate was incubated with either rhotekin-RBD or PAKPBD glutathione beads for 1 h at 4 °C. After washing, the bound proteins were analyzed by western blot with monoclonal antibody against RhoA, Rac1 and Cdc42 to detect GTP-RhoA, GTP-Rac1 and GTP-Cdc42, respectively.

2.14. RNA extraction, reverse transcription and real-time PCR analysis

Total RNA was extracted from cells with the Trizol reagent (Takara, Shiga, Japan) and reverse-transcribed into complementary DNA (cDNA) using 500 ng RNA for qPCR following manufacturer's instructions. miRNA and mRNA levels were quantified using qPCR. U6 and GAPDH mRNAs served as loading controls.

2.15. miRNA transfection

MiR-200b-3p inhibitor was purchased from GenePharma (Shanghai, China). Cells in exponential phase of growth were plated in 60 mm plates at 1×10^6 cells/plate and cultured for 16 h, and then transfected with miR-200b-3p inhibitor or scramble control (100 nM) using HiPerFect transfection reagent according to the manufacturer's instructions (QIAGEN, Shanghai, China).

2.16. Immunofluorescence staining

Cells were seeded onto 12-well glass slides. After treatment, cells were fixed in 4% paraformaldehyde in PBS for 30 min and permeabilized with 0.3% Triton X-100 in PBS for 30 min at room temperature. Slides were then blocked in 2% serum for 1 h and incubated with primary antibodies at 4 °C overnight. After incubation, slides were then washed and incubated with the corresponding secondary antibodies. After three times of PBS washing, slides were mounted for confocal immunofluorescence analysis.

2.17. Statistical analysis

Data represent the mean ± SEM. Statistical significances among groups were tested by a one-way analysis of variance (ANOVA) with post-hoc Tukey tests and comparisons between two groups were evaluated using Student *t*-test. $p < .05$ was considered statistically significant.

3. Results

3.1. GRP78 promoted migration of macrophages

We previously observed secretion of GRP78 from colon cancer cells [10,12] and the serum concentration of GRP78 was up to 40 nM in colon cancer patients [23]. To investigate whether GRP78 secretion was closely correlated with malignant degree of tumors, levels of secreted GRP78 in different types of colon cancer cells were measured. As shown in Fig. 1A, GRP78 secretion occurred in four types of colon cancer cells. Consistently, the content of GRP78 in serums of colon cancer metastatic patients was much higher than that in non-metastatic patients (Fig. 1B). Furthermore, we generated two stable cell lines with over-expressed or reduced GRP78 in DLD1 cell lines. The results showed that DLD1 cells expressing GFP-tagged GRP78 released more GRP78 protein extracellularly compared to GRP78-silenced cells (Fig. 1C). GRP78 and tumor-related macrophages (TAMs) have similar function in the same location of tumor microenvironment. To determine whether GRP78 functions as a potent chemoattractant to recruit macrophages, a series of migration assays were performed to examine the capacity of GRP78 to attract macrophages/monocytes *in vitro* (Schematic diagram shown in Fig. 1D). Tumor conditioned medium (TCM) with different GRP78 secretion was used to attract RAW264.7 cells. As expected, the migration rate was positively correlated with levels of secreted GRP78 (Fig. 1E and F). Furthermore, TCM from GRP78-silenced DLD1 cells dramatically reduced migration of RAW264.7 cells compared with the matched control cells, whereas over-expression of GRP78 significantly increased migration of RAW264.7 cells (Fig. 1G and H). Moreover, GRP78 antibody was used to neutralize GRP78 of TCM, and TCM without secreted GRP78 was applied to detect the effect on macrophage migration. The results of Transwell assays showed that neutralization of GRP78 attenuated migration-promoted effect of TCM on RAW264.7 cells (Fig. 1I and J).

Despite the strong evidence showed that GRP78 facilitated migration of macrophages, it did not rule out the possibility that other secretory factors in CM may influence the cell migration. To further confirm the role of GRP78 in migration of RAW264.7 cells, a recombinant GRP78 protein with His tag (His-GRP78) was used, which could differ from endogenous GRP78 protein. Consistent with the above results, RAW264.7 migration was significantly enhanced in a time/dose-dependent manner in the presence of His-GRP78 (Fig. 2A and B). Consistently, the same phenomenon was observed in THP-1 cell line that could be primed from monocytes to become macrophage-like cells (Fig. 2C and D). Likewise, mBMDMs migration was also evidently enhanced when treated with His-GRP78 (Fig. 2E and F). Wound healing assay revealed that GRP78 also obviously accelerated RAW264.7 cell motility and wound closure rate (Fig. 2G). Collectively, these data demonstrate that GRP78 has a strong capacity to attract macrophages.

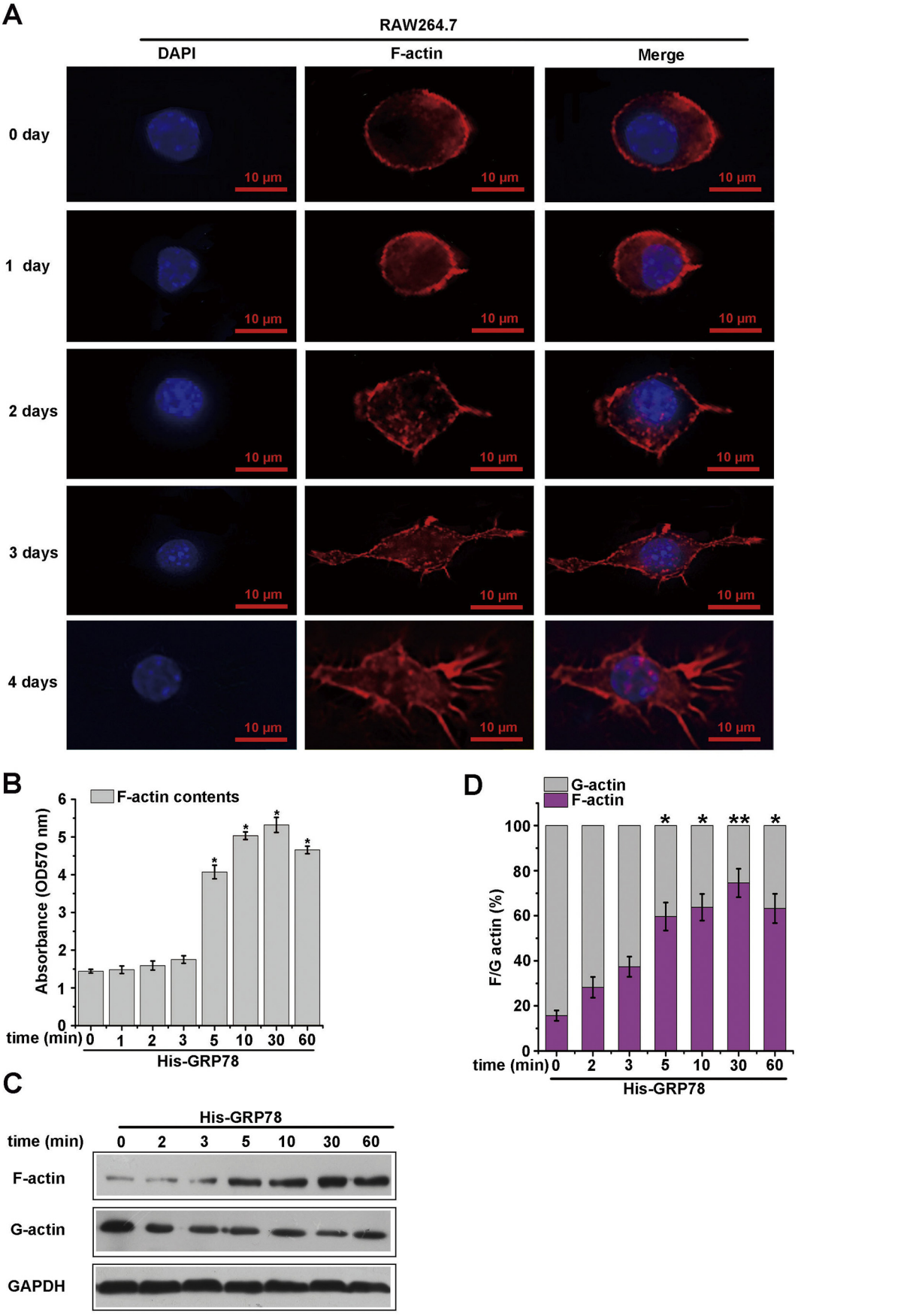

(caption on next page)

Fig. 6. The polarized cell increases F-actin remodeling.
(A) The changes of cytoskeleton in GRP78 gradient-induced RAW264.7 cells. The schematic diagram of experimental design as described in Fig. 3B. Standard confocal sections of RAW264.7 cells treated with secreted GRP78 for 1 day, 2 days, 3 days and 4 days, stained with Phalloidin (red) to mark F-actin, and DAPI (blue) to mark nucleus. Scale bars, 10 μm. (B) RAW264.7 cells were treated with His-GRP78 (40 nM) for different time and F-actin contents were analyzed by detecting the absorbance of Phalloidin in 570 nm. (C) Western blot on protein extracts from RAW264.7 cells treated with His-GRP78 for 2, 3, 5, 10, 30 or 60 min, blotted with anti-actin and anti-GAPDH. (D) Quantification from three biological replicates of the G-actin (grey) and F-actin (purple) ratio in His-GRP78-treated RAW264.7 cells for the same time points indicated as Fig. 6C, normalized to GAPDH for the corresponding lanes on western blots. (For interpretation of the references to colour in this figure legend, the reader is referred to the web version of this article.)

3.2. GRP78 recruited macrophages in vitro and in vivo

To determine whether macrophages migrate in a certain direction, the 3 cycle assays in the 6-well plates were designed (Schematic diagram shown in Fig. 3B). The number of RAW264.7 cells that migrated toward DLD1 cells with over-expressed GRP78 was much greater than that of RAW264.7 cells that moved toward DLD1 cells without over-expressed GRP78 (Fig. 3A). In contrast, the number of RAW264.7 cells that moved toward DLD1 cells with ablated GRP78 was much smaller than that of RAW264.7 cells that migrated toward DLD1-sh-Cont cells (Fig. 3A). Moreover, the migration distance of RAW264.7 toward DLD1 cells with over-expressed GRP78 was 4.5 mm, which was further than the 0.9 mm migration distance of RAW264.7 toward DLD1 control cells. While the distance of RAW264.7 migration toward DLD1 with reduced GRP78 was only 1.2 mm, which was smaller than the 3.0 mm migration distance of RAW264.7 cells to DLD1 control cells (Fig. 3C and D). In summary, GRP78 was able to promote migration of macrophages.

We further evaluated the effect of GRP78 over-expression and silence on macrophage migration in xenografts (Schematic diagram shown in Fig. 3E). The number of $CD68^+$ macrophages was much higher in the mice tumor tissues inoculated with the lenti-GRP78/DLD1 cells than mice transplanted with the lenti-vector/DLD1 cells (Fig. 3F). While mice transplanted with the shGRP78/DLD1 cells showed fewer $CD68^+$ macrophages infiltration in the tumor tissues than that with shNC/DLD1 cells (Fig. 3F).

To further confirm the correlation between GRP78 and macrophages in tumors, immunohistochemical staining of TAM markers (CD68) in the mice matrigel tissues that have various concentrations of GRP78 was performed (Schematic diagram shown in Fig. 3G). The results showed that fraction of $CD68^+$ macrophages that infiltrated into matrigel was markedly increased along with the gradient concentrations of GRP78, confirming a positive correlation between levels of GRP78 and TAM infiltration (Fig. 3H). These data suggested that the migration of macrophages was not irregular, but a directional migration along the GRP78 concentration gradient and macrophage was easier to infiltrate into GRP78-abundant regions.

3.3. GRP78 could combine with intracellular Ca^{2+} and boost RAW264.7 cell polarity

GRP78 is a typical calmodulin, and secreted GRP78 is able to enter into RAW264.7 cells by phagocytosis and clathrin, caveolin-1 and micropinocytosis-mediated endocytosis pathways [23], encouraging us to determine the changes of calcium in the cytosol using fluorescent dye Fluo-3 AM (green) after secreted mCherry-GRP78 (red) into macrophages were examined. As shown in Fig. 4A, intracellular calcium ions in RAW264.7 cells were evenly distributed when the cells were attached on the plate after 4 h. As the culture time increasing, more mCherry-GRP78 was secreted by mCherry-GRP78/DLD1 cells, forming a GRP78 concentration gradient at both sides of RAW264.7 cells compared to mCherry-vector/DLD1 cells. Therefore, DLD1-mCherry-GRP78cells secreted more GRP78 that entered into RAW264.7 cells and bound to Ca^{2+} compared to the corresponding control DLD1-mCherry group. This made intracellular originally uniform free Ca^{2+} present at a heterogeneous distribution in the cells. The further line-scan quantification also revealed that GRP78 and intracellular Ca^{2+} had more similar fluorescence intensity in the same wavelength with the increasing culture time, suggesting that they co-localized in RAW264.7 cells (Fig. 4B–E). All these results demonstrated that the binding of GRP78 to intracellular calcium ions, at least in part, promoted polarity of RAW264.7 cells.

3.4. Polarity of RAW264.7 cells contributed to the ECM adhesion and matrix degradation

Enhanced cell-matrix adhesion is an important step during cancer cell metastasis [24]. To investigate the role of GRP78 in regulating cell-matrix adhesion in RAW264.7 cells, the adherence rate was examined in the presence or absence of GRP78. As shown in Fig. 5A, GRP78 strengthened the adhesion of RAW264.7 cells to the pre-coated collagen layer that mimicked the natural ECM features. From the quantified results, we observed that RAW264.7 cells with GRP78 treatment showed a rapid increase in the proportion of adhesion rate compared to RAW264.7 cells without GRP78 treatment (Fig. 5B). Next, levels of typical pro-adhesion molecules including fibronectin, integrin-β1 and FAK were examined in the presence of GRP78 in RAW264.7 and THP-1 cells. All of immunofluorescence staining, qPCR and western blot assays revealed that GRP78 significantly promoted expression of fibronectin, integrin-β1 and FAK and activated integrin-β1 (12G10) and p-FAK (Tyr397) (Fig. 5C, D, E, F and G). These results suggested that the pro-migratory role of GRP78 was likely ascribed to its adhesion-promoting function.

Degradation of extracellular matrix is a critical step for cell migration. Therefore, we measured expression of two classical molecules MMP-2 and MMP-9. qPCR and western blot revealed an increased levels of MMP-2 and MMP-9 in RAW264.7 and THP-1 cells treated with 40 nM His-GRP78 compared to control group (Fig. 5H–J). Importantly, gelatin zymography analysis also revealed the increased MMP-2 and MMP-9 activity after 40 nM His-GRP78 treatment in RAW264.7 cells (Fig. 5K). Taken together, these findings strongly suggested that GRP78 was involved in enhancing adhesion, ultimately increasing the ability of cells to degrade the surrounding matrix.

3.5. Polarity of macrophages caused reorganization of the actin cytoskeleton

Cytoskeleton rearrangement plays an essential role in chemotaxis [25]. Lenti-GRP78/DLD1 cells and lenti-vector/DLD1 cells secreted GRP78 at a gradient concentration, which enables RAW264.7 cells to migrate in a certain direction. As shown in Fig. 6A, at the beginning of RAW264.7 cells attachment, they showed the round shape. 24 h later, structure of cytoskeleton was slightly changed. On Day 2, basal fibers of actin accumulated, and the shape was not as round at the beginning of attachment, they tended to extend pseudopodia toward lenti-GRP78/DLD1 cells. On Day 3, RAW264.7 cells exhibited markedly polarity such as the front protrusion and rear contraction of the migration, suggesting that the cytoskeleton undergone a severe rearrangement. On Day 4, an obvious cell migration in a certain direction was observed after a large amount of secreted GRP78 induction.

Due to limited numbers of tumor cells and insufficient secretion of GRP78 in the above experiments, we next directly treated macrophages with GRP78 to examine the acute effects of GRP78 on filamentous actin

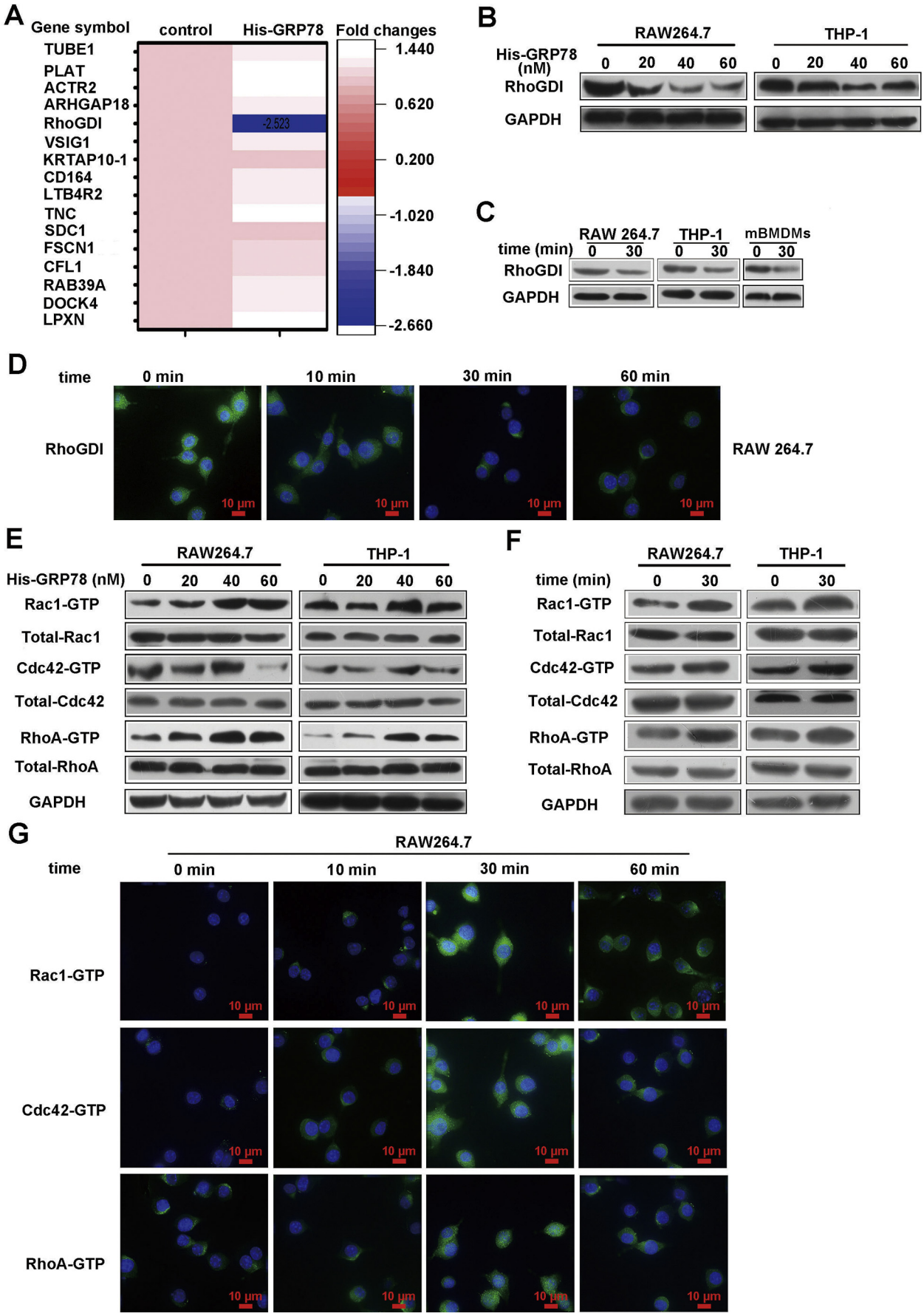

(caption on next page)

Fig. 7. RhoGDIA plays a vital role in GRP78-stimulated cytoskeleton remodeling.
(A) Heatmaps of gene expression in THP-1 cells treated with His-GRP78 for 30 min. Red and blue indicated genes up- and down-regulated, respectively. (B) Western blot was used to analyze the level of RhoGDI protein in RAW264.7 and THP-1 cells treated with indicated concentrations of His-GRP78 for 30 min. (C) RAW264.7, THP-1 and mBMDMs cells were treated with His-GRP78 (40 nM) for 30 min and the level of RhoGDI was detected by western blot. (D) Immune-fluorescence staining was used to detect RhoGDI level in RAW264.7 cells treated with His-GRP78 (40 nM) for different time courses, scale bar represents 10 μm. (E) Pull-down assays for the active RhoA, Rac1, and Cdc42 in RAW264.7 and THP-1 cells treated with different concentrations of His-GRP78 for 30 min. (F) Pull-down assays for the active RhoA, Rac1 and Cdc42 in RAW264.7 and THP-1 cells treated with 40 nM His-GRP78 for 30 min. (G) Immune-fluorescence staining was used to detect active RhoA, Rac1 and Cdc42 levels in RAW264.7 cells treated with His-GRP78, scale bar represents 10 μm. (For interpretation of the references to colour in this figure legend, the reader is referred to the web version of this article.)

(F-actin). The results showed that 5 min of GRP78 treatment led to a significant increase in F-actin, and levels of F-actin reached the maximum at 30 min in RAW264.7 cells as revealed by the rhodamine-phalloidin method (Fig. 6B).

Accumulating evidence suggests that actin is a major structural protein that exists in a monomeric globular form (G-actin) or a polymerized filamentous form (F-actin) composed of aggregated G-actin. G-actin and F-actin forma complex filamentous network provides structural support for cells [26]. The ratio of F-actin to G-actin reflects the balance between actin polymerization and depolymerization. Thus, the actin polymerization, insoluble (F-actin) and soluble (G-actin) fractions of actin were measured by western blot. Similar to the rhodamine-phalloidin results, His-GRP78 treatment caused a significant increase in the ratio of F-actin to G-actin and reached the peak at 30 min, suggesting that GRP78 played an important role in cytoskeleton rearrangement (Fig. 6C and D). These results indicated that GRP78 induced a rapid polymerization of actin filaments in RAW264.7 cells.

3.6. RhoGDIA mediated the role of GRP78 in stimulating cytoskeleton remodeling

GRP78 treatment led to changes of RAW264.7 cell morphology. To define the underlying mechanism for this observance, we determined expression of 16 genes that are involved in cytoskeleton organization. Among the 16 genes, both mRNA and protein levels of RhoGDIA (Rho-specific guanine nucleotide dissociation inhibitor A), a member of RhoGDIs family that control the active-inactive state of RhoGTPases [27], was significantly reduced after His-GRP78 treatment in RAW264.7, THP-1 and mBMDMs (Fig. 7A–C). Furthermore, the fluorescence intensity of RhoGDI was deceased after His-GRP78 treatment (Fig. 7D).

The major function of RhoGDIA inhibits GTPase activity of RhoGTPases proteins. Among these proteins, three of them, RhoA, Rac1 and Cdc42, are well known to regulate cytoskeleton remodeling [28]. We thus examined the effects of GRP78 on the activity and expression of RhoA, Rac1 and Cdc42 in both RAW264.7 and THP-1 cells. Indeed, expression of RhoA, Rac1 and Cdc42 did not show any obvious alteration in both cell lines (Fig. 7E and F). Due to the important role of these three proteins in modifying GTPase activity, we further measured their activities. The results revealed that the activities of RhoA, Rac1 and Cdc42 were significantly increased in both cell lines (Fig. 7E and F). Consistently, immune-staining also revealed increased activities of RhoA, Rac1 and Cdc42 in the presence of His-GRP78, and reached the peak at 30 min in RAW264.7 cells (Fig. 7G).

3.7. RhoGDIA was a direct target of miR-200b-3p

We established that GRP78 reduced mRNA levels of *RhoGDI*. Previous reports showed that microRNAs (miRNAs) are involved in regulation of *RhoGDI* expression [29,30]. To identify miRNAs that regulate *RhoGDIA* expression, three commonly-used prediction algorithms including TargetScan, TarBase and miRNAPath were used to predict miRNAs that have binding site within the 3′ untranslated region (3′ UTR) of *RhoGDIA* gene. TargetScan identified 25 potential miRNAs that potentially target *RhoGDIA*, and 14 and 17 miRNAs were found in the TarBase and miRNAPath datasets respectively that target mouse *RhoGDIA* (Fig. 8A). In addition, 41 miRNAs were predicted to target human *RhoGDIA* by TargetScan, and 102 and 22 miRNAs that potentially target *RhoGDIA* were identified in TarBase and miRNAPath datasets, respectively (Fig. 8B). Only common miRNAs from three prediction approaches were further selected as our targets for experimental verification (Fig. 8A and B). After that, we selected 8 and 16 miRNAs that highly matched and conserved with 3′ UTR of mouse and human *RhoGDIA* to determine their expression in His-GRP78-treated cells (Supplementary Fig. 1A–C and Fig. 8E). The results showed that His-GRP78 treatment altered expression of these miRNAs and we focused on miR-200b-3p because its expression was the most significantly changed in RAW264.7 and THP-1 cells (Fig. 8C and D). Meanwhile, His-GRP78 treatment also led to a sharp increase of miR-200b-3p in mBMDMs (Fig. 8F).

3.8. MiR-200b-3p showed an important role in GRP78-induced migration

Next, we examined activity of RhoGTPases, and the results showed that miR-200b-3p inhibitor treatment led to a sharp increase in RhoGDIA expression that subsequently de-activated RhoA, Rac1 and Cdc42 (Fig. 8G and H). To determine whether miR-200b-3p was involved in the directional migration of macrophages treated with GRP78, the migration of RAW264.7 and THP-1 transfected with miR-200b-3p inhibitor were measured. The results showed that miR-200b-3p knockdown inhibited migration of RAW264.7 and THP-1 cells (Fig. 8I and J). These results demonstrated that GRP78 treatment led to up-regulated expression of miR-200b-3p expression and down-regulated of RhoGDIA, which increased the activities of Rho GTPases and facilitated migration of macrophages.

4. Discussion

It is widely recognized that macrophages represent a prominent component in most malignant tumors and in some instances can comprise up to 50% of the cell tumor mass [31,32]. These cells, often called tumor-associated macrophages (TAMs), are thought to be accumulated in hypoxic areas of tumors [33–36]. Several hypotheses have proposed how TAMs are recruited to and retained in the hypoxic tumor microenvironment. The mechanisms mainly include hypoxia-mediated up-regulation of chemo-attractants and down-regulation of chemokine receptors. For instance, TAMs may be induced in hypoxic areas to secrete chemo-attractants such as EMAPII, endothelin and VEGF-A, and thus attract more TAMs to these areas [37]. On the other hand, hypoxia also restrains macrophages by decreasing their mobility through the up-regulation of MKP-1 enzymes, and this terminates the macrophage response to chemo-attractants outside the hypoxic areas [38]. Most of the studies focus on how the fraction of macrophages that have migrated to the center of tumor tissue stimulated other macrophages to infiltrate into this area. Up to date, the mechanism by which the primary macrophages infiltrate into tumors is poorly described. Our findings revealed that GRP78 concentration gradient was formed in the tumor tissue center and para-cancerous tissues led to the tendency of macrophage migration into tumor tissues. Our findings provided a novel insight into the mechanism of infiltration of macrophages into tumors. Moreover, published literatures focus on the recruit role of chemical attractants secreted by macrophages themselves to other macrophages,

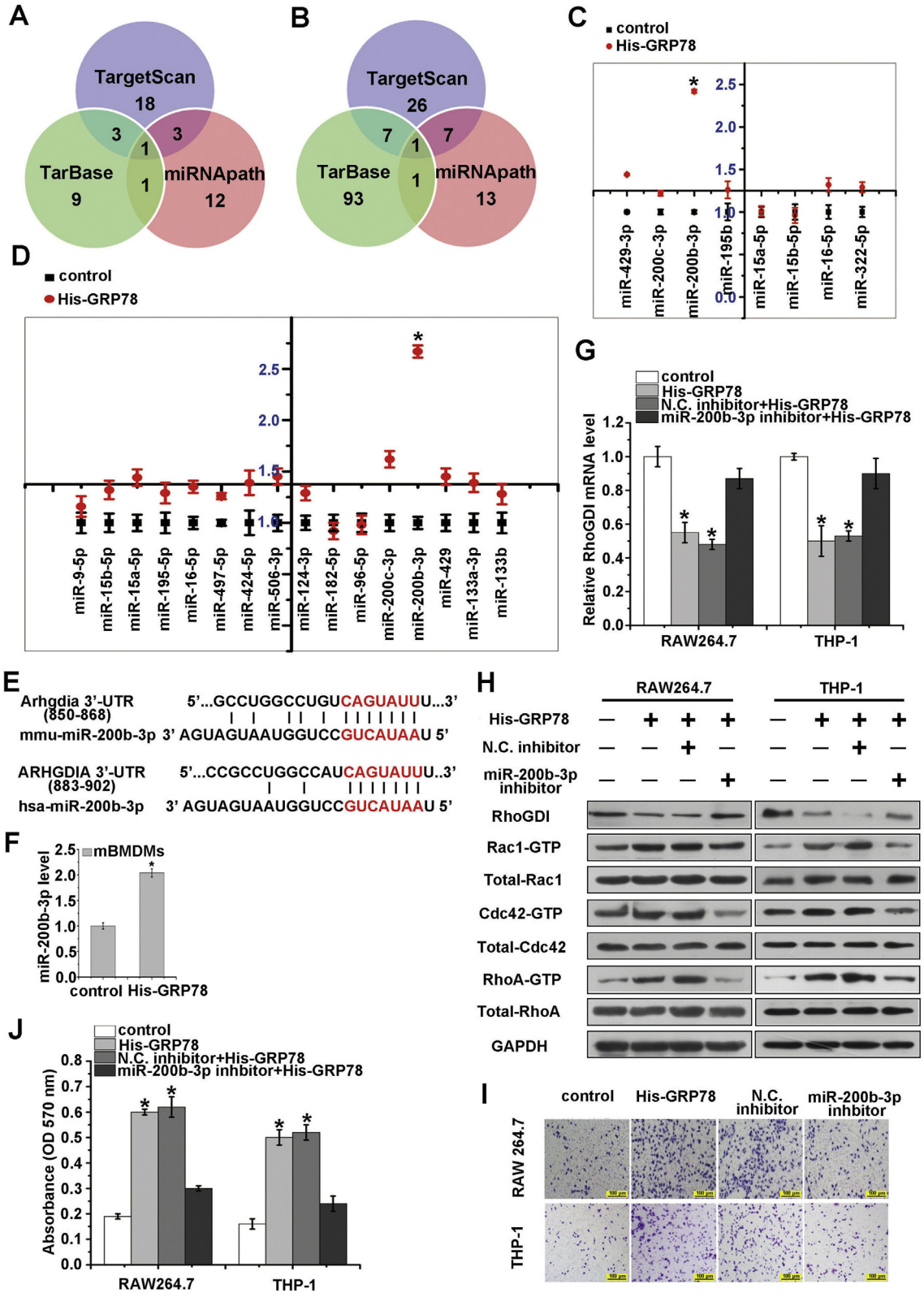

Fig. 8. MiR-200b-3p take an important role in GRP78-induced migration of RAW264.7 and THP-1 cells.
(A-B) The miRNAs that targeting mouse (A) and human (B) *RhoGDI* gene 3′ UTR conserved region were predicted by using online TargetScan, TarBase and miRNApath databases and the co-regulated miRNAs were screened by VENNY tool. (C and D) Endogenous expression of eight and sixteen candidates miRNAs was determined by quantitative real-time PCR analysis in RAW264.7 (C) and THP-1 (D) cells and normalized to U6 snRNA. (E) The sequence of regions of the mouse and human *RhoGDI* 3′-UTR showing complementary pairing with confirmed candidates miR-200b-3p. (F) miR-200b-3p level was detected in mBMDMs in the presence of His-GRP78, $^{*}p < .05$. (G) RhoGDI expression was analyzed by qPCR after RAW264.7 and THP-1 cells transfected with miR-200b-3p inhibitor in the presence or absence of His-GRP78. Data were representative of at least three independent experiments. (H) Pull-down assays for the active RhoA, Rac1 and Cdc42 and western blot assays for the RhoGDI expression in RAW264.7 and THP-1 cells transfected with miR-200b-3p inhibitor in the presence or absence of His-GRP78. (I and J) miR-200b-3p inhibitor was applied to evaluate the effects on RAW264.7 and THP-1 cells migration by Transwell assay. Scale bar represented 100 μm. The bar graph represented the cell motility as shown in (I) $^{*}p < .05$.

while the role of chemokines released by tumor cells in attracting macrophage is rarely described. Our research revealed that GRP78 secreted by tumor cells acted as a chemokine to recruit macrophages into tumor tissues.

GRP78 is well described as a prognostic biomarker of colorectal cancer (CRC) [4], and has been investigated as a serum and histological diagnostic biomarker for gastric cancer alike [39], indicating that tumor-secreted GRP78 may play a vital role in tumor progression. Our previous study demonstrated that secreted GRP78 facilitated the differentiation of BMSCs into CAFs [12]; and the findings in this study revealed a novel function of secreted GRP78 to facilitate the migration of macrophage into tumor tissues without obvious effect on macrophage proliferation (Supplementary Fig. 2A and B). All these findings suggest that secreted GRP78 has a potent transform role for tumor microenvironment. Furthermore, it is well-known that tumor vasculature is essential for tumor growth and survival. Johann Kern et al. revealed that tumor-secreted GRP78 promoted angiogenesis by facilitating the proliferation of HUVEC cells [11]. Therefore, we speculate that secreted GRP78 can also be used as a chemokine to recruit endothelial cells into tumor vasculature and promote tumor progression based on the same mechanisms as macrophages. However, the relationship and regulatory mechanisms between GRP78 and endothelial cells are poorly described and further investigation is needed.

In addition to extracellular chemo-attractant stimuli, directional cell movement depends on an intracellular calcium signal that is organized in space, time and concentration [40–42]. Alteration of Ca^{2+} homeostasis is known to regulate many tumoral processes including proliferation, migration, focal adhesion turnover, FAK activation or transcriptional activity [43,44]. Here, we revealed the entrance of GRP78 into macrophages combined with intracellular Ca^{2+}, which caused change of free Ca^{2+} concentration and further made intracellular calcium display a rear-to-front gradient. In cells moving persistently in one direction, $[Ca^{2+}]$ was highest at the rear and lowest at the front of the cell. It was consistent with Fay and colleagues' previous observations [41]. The concentration of intracellular free calcium ($[Ca^{2+}]$) in polarized macrophages was imaged during chemotaxis (Fig. 3). All these changes in $[Ca^{2+}]$ provide a basis for producing the cell polarization, and polarity is the foundation for cell migration.

Due to the important role of cytoskeletal remodeling in cell migration, in this study, we investigated expression alteration of 16 genes that are involved in and frequently occurred in cytoskeleton organization (Fig. 7A). Of these genes, expression change of RhoGDIA is the highest variation after His-GRP78 treatment and this observation have also been reported to be involved in a wide variety of human symptoms [45,46]. Deregulation of RhoGDIA also occurs in human cancers such as lung cancer [47] and breast cancer [48]. Previous studies showed that regulation of RhoGDIA was mainly restricted at the post-translational level by phosphorylation [49]. To better understand the molecular mechanism of RhoGDIA decrease by GRP78, we combined three online algorithms (as described in Materials and methods) and VENNY tool to predict the miRNAs that target 3′ UTR of *RhoGDIA*. Levels of these candidate miRNAs were measured by qPCR, and miR-200b-3p was the most elevated, which further decreased the expression of *RhoGDIA* at both the mRNA and protein levels in the presence of His-GRP78 (Fig. 8G and H), thus providing a new line of evidence of expression regulation of RhoGDIA at the post-transcriptional level by miRNA. This inhibitory effect might work synergistically with fibronectin/integrin-β1/FAK signaling (Fig. 5) to promote cell motility and invasion. It has been reported that Rho GTPase might be regulated by RhoGDIs, which prevents nucleotide exchange and membrane association of Rho GTPases and thus blocked their activation [50]. Consistent with findings from other studies, our results showed that inhibition of RhoGDIA activated Rac1, Cdc42 and RhoA (Fig. 7). Anne J. Ridley's showed that protruding leading edge is initially determined by Cdc42- and Rac-mediated polarization and actin polymerization and Rho-mediated actomyosin contraction [51], and combining with our study, we suspect that GRP78 made GTP-Rac1, GTP-Cdc42 distributed in front protrusion and GTP-RhoA located in rear contraction, further guiding macrophage directional migration. Together, these findings demonstrate that RhoGDIA plays an important role in GRP78 gradient-induced macrophage recruitment.

5. Conclusions

The gradient of chemoattractant-GRP78 initiates changes calcium distribution that activates calcium-dependent effector proteins, RhoA, Rac1 and Cdc42, which further causes local cytoskeletal remodeling, imbalance of membrane tension and asymmetric protrusion. These subcellular changes finally result in directional migration of macrophage. This finding not only uncovers a new function of GRP78 secreted by tumor cells, but also provides a reasonable explanation for the primary macrophage migrated to tumor tissue.

Supplementary data to this article can be found online at https://doi.org/10.1016/j.cellsig.2019.04.004.

Conflict of interest statement

The authors declare no conflict of interest.

Author contributions

X.Q.L. and Z.Y.L. provided the initial concept. X.Q.L. performed the majority of the experiments and collected the data and wrote the initial draft of the manuscript. L.C.Z. performed the data analysis and interpretation. Y.F.Y. performed the qRT-PCR and western blot assays. H.Q.L. performed the *in vivo* experiments and participated in study design and coordination. Z.Y.L. and G.S.S. revised the manuscript repeatedly. All authors read and approved the final manuscript.

Acknowledgement

This work was supported by the National Natural Science Foundation of China (No. 31770382 and No. 81803791), '1331 project' Collaborative Innovation Center and team (1331 CIC), Shanxi Province Science Foundation for Youths (201801D221249), Key Project of Shanxi Province (201801D111001).

References

[1] A.S. Lee, The glucose-regulated proteins: stress induction and clinical applications, Trends Biochem. Sci. 26 (8) (2001) 504–510.
[2] G. Zhu, A.S. Lee, Role of the unfolded protein response, GRP78 and GRP94 in organ homeostasis, J. Cell. Physiol. 230 (7) (2015) 1413–1420.
[3] L.H. Zhang, X. Zhang, Roles of GRP78 in physiology and cancer, J. Cell. Biochem. 110 (6) (2010) 1299–1305.
[4] A.S. Lee, GRP78 induction in cancer: therapeutic and prognostic implications, Cancer Res. 67 (8) (2007) 3496–3499.
[5] M. Ni, A.S. Lee, ER chaperones in mammalian development and human diseases, FEBS Lett. 581 (19) (2007) 3641–3651.
[6] F.M. Uckun, S. Qazi, Z. Ozer, A.L. Garner, J. Pitt, H. Ma, K.D. Janda, Inducing apoptosis in chemotherapy-resistant B-lineage acute lymphoblastic leukaemia cells by targeting HSPA5, a master regulator of the anti-apoptotic unfolded protein response signalling network, Br. J. Haematol. 153 (6) (2011) 741–752.
[7] W.T. Chen, G. Zhu, K. Pfaffenbach, G. Kanel, B. Stiles, A.S. Lee, GRP78 as a regulator of liver steatosis and cancer progression mediated by loss of the tumor suppressor PTEN, Oncogene 33 (42) (2014) 4997–5005.
[8] M. Ni, Y. Zhang, A.S. Lee, Beyond the endoplasmic reticulum: atypical GRP78 in cell viability, signalling and therapeutic targeting, Biochem. J. 434 (2) (2011) 181–188.
[9] D. Dong, C. Stapleton, B. Luo, S. Xiong, W. Ye, Y. Zhang, N. Jhaveri, G. Zhu, R. Ye, Z. Liu, K.W. Bruhn, N. Craft, S. Groshen, F.M. Hofman, A.S. Lee, A critical role for GRP78/BiP in the tumor microenvironment for neovascularization during tumor growth and metastasis, Cancer Res. 71 (8) (2011) 2848–2857.
[10] Z. Li, M. Zhuang, L. Zhang, X. Zheng, P. Yang, Z. Li, Acetylation modification regulates GRP78 secretion in colon cancer cells, Sci. Rep. 6 (2016) 30406–30416.
[11] J. Kern, G. Untergasser, C. Zenzmaier, B. Sarg, G. Gastl, E. Gunsilius, M. Steurer, GRP-78 secreted by tumor cells blocks the antiangiogenic activity of bortezomib, Blood 114 (18) (2009) 3960–3967.
[12] Y. Peng, Z. Li, Z. Li, GRP78 secreted by tumor cells stimulates differentiation of

bone marrow mesenchymal stem cells to cancer-associated fibroblasts, Biochem. Biophys. Res. Commun. 440 (4) (2013) 558–563.
[13] F. Ginhoux, S. Jung, Monocytes and macrophages: developmental pathways and tissue homeostasis, Nat. Rev. Immunol. 14 (6) (2014) 392–404.
[14] N.B. Hao, M.H. Lu, Y.H. Fan, Y.L. Cao, Z.R. Zhang, S.M. Yang, Macrophages in tumor microenvironments and the progression of tumors, Clin. Dev. Immunol. 2012 (2012) 948098–948108.
[15] A. Casazza, D. Laoui, M. Wenes, S. Rizzolio, N. Bassani, M. Mambretti, S. Deschoemaeker, J.A. Van Ginderachter, L. Tamagnone, M. Mazzone, Impeding macrophage entry into hypoxic tumor areas by Sema3A/Nrp1 signaling blockade inhibits angiogenesis and restores antitumor immunity, Cancer Cell 24 (6) (2013) 695–709.
[16] A. Sica, A. Saccani, B. Bottazzi, S. Bernasconi, P. Allavena, B. Gaetano, F. Fei, G. LaRosa, C. Scotton, F. Balkwill, A. Mantovani, Defective expression of the monocyte chemotactic Protein-1 receptor CCR2 in macrophages associated with human ovarian carcinoma, J. Immunol. 164 (2) (2000) 733–738.
[17] M.J. Grimshaw, F.R. Balkwill, Inhibition of monocyte and macrophage chemotaxis by hypoxia and inflammation – a potential mechanism, Eur. J. Immunol. 31 (2) (2001) 480–489.
[18] N.D. Staudt, M. Jo, J. Hu, J.M. Bristow, D.P. Pizzo, A. Gaultier, S.R. VandenBerg, S.L. Gonias, Myeloid cell receptor LRP1/CD91 regulates monocyte recruitment and angiogenesis in tumors, Cancer Res. 73 (13) (2013) 3902–3912.
[19] M. Tanaka, S. Shimamura, S. Kuriyama, D. Maeda, A. Goto, N. Aiba, SKAP2 promotes Podosome formation to facilitate tumor-associated macrophage infiltration and metastatic progression, Cancer Res. 76 (2) (2016) 358–369.
[20] T. Hagemann, S.C. Robinson, M. Schulz, L. Trumper, F.R. Balkwill, C. Binder, Enhanced invasiveness of breast cancer cell lines upon co-cultivation with macrophages is due to TNF-a dependent up-regulation of matrix metalloproteases, Carcinogenesis 25 (8) (2004) 1543–1549.
[21] F.J. Rios, R.M. Touyz, A.C. Montezano, Isolation and differentiation of murine macrophages, Methods Mol. Biol. 1527 (2017) 297–309.
[22] X. La, L. Zhang, Z. Li, P. Yang, Y. Wang, Berberine-induced autophagic cell death by elevating GRP78 levels in cancer cells, Oncotarget 8 (13) (2017) 20909–20924.
[23] X. La, L. Zhang, H. Li, Z. Li, G. Song, P. Yang, Y. Yang, Ajuba receptor mediates the internalization of tumor-secreted GRP78 into macrophages through different endocytosis pathways, Oncotarget 9 (21) (2018) 15464–15479.
[24] T.R. Geiger, D.S. Peeper, Metastasis mechanisms, Biochim. Biophys. Acta 1796 (2) (2009) 293–308.
[25] T.D. Pollard, G.G. Borisy, Cellular motility driven by assembly and disassembly of actin filaments, Cell 112 (4) (2003) 453–465.
[26] L.A. Cingolani, Y. Goda, Actin in action: the interplay between the actin cytoskeleton and synaptic efficacy, Nat. Rev. Neurosci. 9 (5) (2008) 344–356.
[27] J.L. Bos, H. Rehmann, A. Wittinghofer, GEFs and GAPs: critical elements in the control of small G proteins, Cell 129 (5) (2007) 865–877.
[28] N. Tapon, A. Hall, Rho, Rac and Cdc42 GTPases regulate the organization of the actin cytoskeleton, Curr. Opin. Cell Biol. 9 (1) (1997) 86–92.
[29] J. Ding, S. Huang, S. Wu, Y. Zhao, L. Liang, M. Yan, C. Ge, J. Yao, T. Chen, D. Wan, H. Wang, J. Gu, M. Yao, J. Li, H. Tu, X. He, Gain of miR-151 on chromosome 8q24.3 facilitates tumour cell migration and spreading through downregulating RhoGDIA, Nat. Cell Biol. 12 (4) (2010) 390–399.
[30] D. Liang, Z. Wang, Z. Yan, S. Hou, W. Xu, L. Wang, M. Shang, Z. Qiao, Nicotine facilitates VSMC dysfunction through a miR-200b/RhoGDIA/cytoskeleton module, Sci. Rep. 7 (2017) 43798–43812.
[31] P.M.A. Kelly, R.S. Davision, E. Bliss, J.O.D. McGee, Macrophages in human breast disease: a quantitative immunohistochemical study, Br. J. Cancer 57 (1988) 174–177.
[32] R.D. Leek, A.L. Harris, C.E. Lewis, Cytokine networks in solid human tumors: regulation of angiogenesis, J. Leukoc. Biol. 56 (1994) 423–435.
[33] R.P.M. Negus, G.W.H. Stamp, J. Hadley, F.R. Balkwill, Quantitative assessment of the leukocyte infiltrate in ovarian cancer and its relationship to the expression of C-C chemokines, Am. J. Pathol. 150 (1997) 1723–1734.
[34] R.D. Leek, C.E. Lewis, R. Whitehouse, M. Greenall, J. Clarke, A.L. Harris, Association of macrophage infiltration with angiogenesis and prognosis in invasive breast carcinoma, Cancer Res. 56 (1996) 4625–4629.
[35] R.D. Leek, R.J. Landers, A.L. Harris, C.E. Lewis, Necrosis correlates with high vascular density and focal macrophage infiltration in invasive carcinoma of the breast, Br. J. Cancer 79 (1999) 991–995.
[36] J.S. Lewis, R.J. Landers, J.C.E. Underwood, A.L. Harris, C.E. Lewis, Expression of vascular endothelial growth factor by macrophages is up-regulated in poorly vascularized areas of breast carcinomas, J. Pathol. 192 (2000) 150–158.
[37] C. Murdoch, A. Giannoudis, C.E. Lewis, Mechanisms regulating the recruitment of macrophages into hypoxic areas of tumors and other ischemic tissues, Blood 104 (8) (2004) 2224–2234.
[38] T. Chanmee, P. Ontong, K. Konno, N. Itano, Tumor-associated macrophages as major players in the tumor microenvironment, Cancers (Basel) 6 (3) (2014) 1670–1690.
[39] Tanigawa, Proteomics-based identification of a tumor-associated antigen and its corresponding autoantibody in gastric cancer, Oncol. Rep. 23 (4) (2010).
[40] P. Friedl, K. Wolf, Plasticity of cell migration: a multiscale tuning model, J. Cell Biol. 188 (1) (2010) 11–19.
[41] K.E.F. Rodney A. Brundage, Richard A. Tuft, Fredric S. Fay, Calcium gradients underlying polarization and chemotaxis of eosinophils, Science 254 (5032) (1991) 703–706.
[42] A.I. Juliet Lee, Gerry Oxford, Barry Johnson, Ken Jacobson, Regulation of cell movement is mediated by stretch-activated calcium channels, Nature 400 (1999) 382–386.
[43] Y.F. Chen, Y.T. Chen, W.T. Chiu, M.R. Shen, Remodeling of calcium signaling in tumor progression, J. Biomed. Sci. 20 (23) (2013) 1–10.
[44] N. Prevarskaya, R. Skryma, Y. Shuba, Calcium in tumour metastasis: new roles for known actors, Nat. Rev. Cancer 11 (8) (2011) 609–618.
[45] A. Togawa, J. Miyoshi, H. Ishizaki, M. Tanaka, A. Takakura, H. Nishioka, H. Yoshida, T. Doi, A. Mizoguchi, N. Matsuura, Y. Niho, Y. Nishimune, S. Nishikawa, Y. Takai, Progressive impairment of kidneys and reproductive organs in mice lacking Rho GDIα, Oncogene 18 (1999) 5373–5380.
[46] R. Maddala, L.W. Reneker, B. Pendurthi, P.V. Rao, Rho GDP dissociation inhibitor-mediated disruption of Rho GTPase activity impairs lens fiber cell migration, elongation and survival, Dev. Biol. 315 (1) (2008) 217–231.
[47] F.H. Blackhall, D.A. Wigle, I. Jurisica, M. Pintilie, N. Liu, G. Darling, M.R. Johnston, S. Keshavjee, T. Waddell, T. Winton, F.A. Shepherd, M.S. Tsao, Validating the prognostic value of marker genes derived from a non-small cell lung cancer microarray study, Lung Cancer 46 (2) (2004) 197–204.
[48] W.G. Jiang, G. Watkins, J. Lane, G.H. Cunnick, A.D. Jones, K. Mokbel, R.E. Mansel, Prognostic value of rho GTPases and rho guanine nucleotide dissociation inhibitors in human breast cancers, Clin. Cancer Res. 9 (2003) 6432–6440.
[49] C. DerMardirossian, A. Schnelzer, G.M. Bokoch, Phosphorylation of RhoGDI by Pak1 mediates dissociation of Rac GTPase, Mol. Cell 15 (1) (2004) 117–127.
[50] A. Dovas, J.R. Couchman, RhoGDI: multiple functions in the regulation of rho family GTPase activities, Biochem. J. 390 (2005) 1–9 Pt 1.
[51] A.J. Ridley, Life at the leading edge, Cell 145 (7) (2011) 1012–1022.